Optimization of Deposition Parameters for α-Al$_2$O$_3$ Coatings by Double Glow Plasma Technique

Y.-B. Lin,[a,b] Y.-Z. Shen,[a] T.-F. Chen,[a] and J. Tao[a*]

[a] College of Material Science and Technology, Nanjing University of Aeronautics and Astronautics, 29 Yudao Street, 210 016 Nanjing, P.R. China

[b] Jiangsu Provincial Key Laboratory for Interventional Medical Devices, Huaiyin Institute of Technology, 1 Meicheng Street, 223 003 Huaian, P.R. China

‖ **Abstract**
The parameters to prepare α-Al$_2$O$_3$ coatings by double glow plasma technique were optimized to obtain dense and thick α-Al$_2$O$_3$ coatings on 316 L stainless steel at low temperature of 580 °C. The parallel distance between the source electrode and the substrate, working pressure, source electrode voltage, and workpiece electrode voltage were designed by L9 Orthogonal array design. The thickness, microstructure, chemical composition and phase components of the sputter-deposited Al/α-Al$_2$O$_3$ coatings were analysed by means of 3-D non-contact surface profiler analysis, scanning electron microscopy equipped with energy dispersive X-ray spectrometry and glancing-angle X-ray diffraction, respectively. The results indicated that the parallel distance between the source electrode and the substrate played a dominant role in determining the thickness of the films. The coatings prepared at the optimum parameters exhibited a very dense, uniform, and compact microstructure without any cracks and defects. It was found that iron aluminide formed at the interface between the coatings and the substrates. The thickness of the coatings reached about 11.6 μm at the deposition rate of ∼64.4 nm min⁻¹. The oxidized coatings with the lowest porosity about 0.13 % had relative content of α-Al$_2$O$_3$ as high as 66.5 % when oxygen flow was 2 sccm.

Introduction

Alumina (Al$_2$O$_3$) has been of great interest in the past few years owing to its excellent properties. Al$_2$O$_3$ is widely used in numerous applications, such as wear resistant coatings for cutting tools,[1] corrosion resistance for magnesium alloy,[2] an insulating layer for semiconductor devices,[3] moisture permeation barrier coatings for porous papers,[4] oxygen permeation barrier coatings for aeronautics and astronautics,[5] or a hydrogen permeation barrier coating for nuclear fusion reactors.[6]

Al$_2$O$_3$ has a number of polymorphs, including κ-phase, γ-phase, θ-phase, α-phase etc. Among the various crystal structures of alumina, the metastable phase tends to transform into the stable one. Thermodynamically stable α-Al$_2$O$_3$ with corundum structure is considered as protective coating on substrates to be used at high temperatures. Generally, it can be deposited using chemical vapour deposition (CVD), physical vapour deposition (PVD), pulsed laser deposition (PLD) as well as magnetron sputtering (MS). Normally, α-alumina coatings can be obtained when the substrate temperature is above 1000 °C in the CVD pro-

cess.[7–9] However, this causes unwanted effects limiting the application of substrate materials, such as steel and glass,[7] and cracks owing to thermal expansion mismatch,[10] which can be avoided by reactive diffusion through post-deposition annealing. Meanwhile, post deposition oxidation after direct Al deposition on 316 L stainless is an efficient way to form (Al$_2$O$_3$ + Fe$_2$O$_3$) interface layers.[11]

It is possible to lower substrate temperature even more by increasing the kinetic energy and controlling flux of the depositing species. α-Al$_2$O$_3$ films on silicon or graphite substrate were deposited by filtered vacuum arc method at substrate temperature of 780 °C according to Y-Yamada-Takamura's study.[12] With a negative bias voltage of 200 V, it was possible to deposit films containing α-Al$_2$O$_3$ with pre-heating the substrate to a lower temperature of 460 °C. A similar result was obtained by Wallin's research,[13] in which α-Al$_2$O$_3$ coatings were deposited directly onto the hard alloy and molybdenum substrates at low temperature (650 °C) using high energetic ion bombardment (20 eV – 100 eV). The above-discussed experiments demonstrated that the crystalline growth temperature of α-Al$_2$O$_3$ could be reduced through energetic ion bombardment. Another interesting approach to synthesize the α-Al$_2$O$_3$ at lower temperatures is based on the utilization of additive elements. Jin et al.[14] and Andersson et al.[15] both

* Corresponding author: Professor Jie Tao
  e-mail: taojie@nuaa.edu.cn

reported the use of an α-Cr_2O_3 template layer for the low temperature growth of α-Al_2O_3 films, and the crystallization temperatures decreased to 600 and 500 °C, respectively. The existence of α-Cr_2O_3 can provide more nucleation sites and decrease the surface energy in the nucleation and growth processes owing to the greatly similar crystalline character.

The double glow plasma technique, a hybrid plasma surface treatment technique, is the combination of the plasma and sputtering processes developed for the deposition of high quality alloyed layers on the surface of inexpensive materials. In this study, double glow plasma technique[16] was used to prepare the high content and well-bonded α-Al_2O_3 coatings on 316 L stainless steel at low temperature of 580 °C. The effects of different factors on the formation of Al_2O_3 coatings are discussed in detail.

Experimental

Materials and methods

A complex target (the composition was Al 90 %, α-Al_2O_3 10 % in weight percent) plate (50 mm × 6 mm) was used as the source electrode for supplying the alloying elements. 316 L stainless steel plate of size 10 mm × 10 mm × 3 mm was used as the substrate material and its nominal composition is shown in Table 1. The specimens were first polished by 1000 grit SiC paper and then cleaned in acetone prior to double-glow plasma surface alloying treatments.

Table 1   – Chemical composition of 316 L stainless steel
Tablica 1 – Kemijski sastav nehrđajućeg čelika 316 L

Chemical element Kemijski element	w / %	Chemical element Kemijski element	w / %
Cr	16.936	Mo	2.215
Ni	10.128	S	0.001
Mn	1.716	P	0.032
Si	0.229	N	0.046
C	0.027	Fe	68.670

A detailed description of double glow plasma apparatus is reported elsewhere.[17] The apparatus had three electrodes: the anode (the shelter) and two negatively cathodes. One cathode was the source cathode (referring to the complex target), and the other cathode was the substrate material.

The source electrode voltage was set at 600–800 V and workpiece electrode voltage was set at 300–400 V. When two different voltages were applied to the two cathodes, glow discharge could be produced. The chamber was evacuated to a base pressure of $2 \cdot 10^{-4}$ Pa. During the deposition process, the flow rates of argon were kept at 40 sccm, where the working pressure was maintained at 20–40 Pa. The parallel distance between the substrate and target was about 10–20 mm with deposition time of 3 h.

Orthogonal array design is a highly efficient method to investigate the relationship between the effects of different factors.[18] As working pressure, source electrode, workpiece electrode and parallel distance would likely influence the deposition rate, three levels were selected for each factor (Table 2), which were fixed in the probable working range. These factors did not play an independent role in the process of the sputtering deposition. Therefore, it is a better choice to study the deposition parameters by orthogonal array design,[19,20] which was applied to evaluate the influences of different factors on the deposition rate. After deposition, the coatings with the optimize parameters were further plasma oxidized through different oxidation environment. The flow rates of argon were kept at 40 sccm while the oxygen flow rates were set in the range of 0.5–4 sccm. The source electrode voltage was set at -700 V and workpiece electrode voltage was set at -300 V to keep the desired temperature of 580 °C. By controlling the mechanical pump, the total pressure of Ar + O_2 was kept at 40 Pa and the oxidization time was 1 h.

Table 2   – Parameters and levels for L9 Orthogonal array design
Tablica 2 – Parametri i razine za dizajn ortogonalnog rasporeda L9

Parameter Parametar	Level 1 Razina 1	Level 2 Razina 2	Level 3 Razina 3
working pressure / Pa radni tlak / Pa	20	30	40
source electrode voltage / V napon izvorne elektrode / V	600	700	800
workpiece electrode voltage / V napon elektrode radnog komada / V	300	350	400
electrode distance / mm udaljenost elektroda / mm	10	15	20

Characterizations

The phase composition of the prepared coatings was characterized with glancing-angle (1°) X-ray diffractometry (GAXRD, UltimaIV, Rigaku Company, CuKα radiation, Japan) operating at 50 kV and 40 mA. X-ray data were collected using a 0.02° step scan with a count time of 8 s. The morphology and chemical composition of the as-deposited coatings were studied by scanning electron microscopy (SEM, Quanta250, FEI Company, US) with an X-ray energy-dispersive spectroscopy (EDS, EDAX Inc. US). In order to measure the thickness of the coatings, one step was prepared by partly blocking the atoms sputtering on the substrate. A micro-XAM surface mapping microscope (Micro-XAM, ADE Phase-Shift, USA), which could present the three-dimensional shape of the coatings was used to measure the thickness of the coatings. Finally, the electrochemical corrosion behaviours of the composite coatings and 316 L stainless steel were characterized by potentiodynamic polarization, which was carried out on a CHI660d electrochemical analyser (Shanghai, China) in aqueous solution, $w(NaCl) = 3.5$ %.

Table 3 – Orthogonal design and experiment results
Tablica 3 – Ortogonalni dizajn i eksperimentalni rezultati

Exp. No. Eksp. br.	Working pressure/Pa Radni tlak/Pa	Source electrode voltage/V Napon izvorne elektrode/V	Workpiece electrode voltage/V Napon elektrode radnog komada/V	Electrode distance/mm Udaljenost elektroda/mm	Thickness/µm Debljina/µm
S1	20	600	300	10	4.4
S2	20	700	350	15	11.8
S3	20	800	400	20	2.0
S4	30	600	350	20	7.0
S5	30	700	400	10	11.8
S6	30	800	300	15	15.6
S7	40	600	400	15	8.5
S8	40	700	300	20	5.3
S9	40	800	350	10	10.0

Table 4 – Analysis of range and optimal parameters
Tablica 4 – Analiza raspona i optimalni parametri

Parameters Parametri	Working pressure/Pa Radni tlak/Pa	Source electrode voltage/V Napon izvorne elektrode/V	Workpiece electrode voltage/V Napon elektrode radnog komada/V	Electrode distance/mm Udaljenost elektroda/mm
K_1	6.1	6.6	8.4	8.7
K_2	11.5	9.6	9.6	12.0
K_3	7.9	9.2	7.4	4.8
R	5.4	3.0	2.2	7.2

Results and discussion

Thickness and the morphology of the coatings

The L9(3^4) table of orthogonal design was used to test the deposition rate under the assigned conditions (Table 3). The thickness of the coatings is taken as measured responses. The range analysis values are presented in Table 4.

R is defined as: $R = \max\{|K_1 - K_2|, |K_2 - K_3|, |K_3 - K_1|\}$. K_i is the mean value around the corresponding index of the thickness column factor. In other words, each cell in this table is of average thickness with one of the deposition parameters kept constant. For example, K_{11} is average value of thickness when working pressure is 20 Pa, while other parameters are varied. Then, $K_{11} = (4.4 + 11.8 + 2)$ / 3 = 6.1. Theoretically, the R value reflects the impact of the corresponding factor on the film properties. The greater the R value, the larger the impact degree.[19] It can be obtained from Table 4 that the parallel distance between the source electrode and the substrate plays the dominant role in the thickness of the films. The optimum parameters are working pressure, 30 Pa; source electrode voltage, 700 V; workpiece electrode voltage, 300 V; the parallel distance between the source electrode and the substrate, 15 mm.

Fig. 1 shows typical surface micrographs of ion sputtering coating samples (unoxidized coatings). It can be seen that sample S1 has some cracks and epidermal desquamation scrape. Sample S3 has some defects by suffering from spalling, so does sample S6. The surface micrographs of the samples S5 and S9 are similar to S1, which results from the mismatch of different thermal expansion coefficients of the materials caused by hollow cathode effect.[21] When the parallel distance between the source electrode and the substrate is too small (10 mm), the overlapping glow current increases sharply, which will result in a high temperature of substrate or sputtering target in the local area. Owing to the temperature gradient existing in the different area of the coatings,[22] cracks and epidermal desquamation scrape can be found.
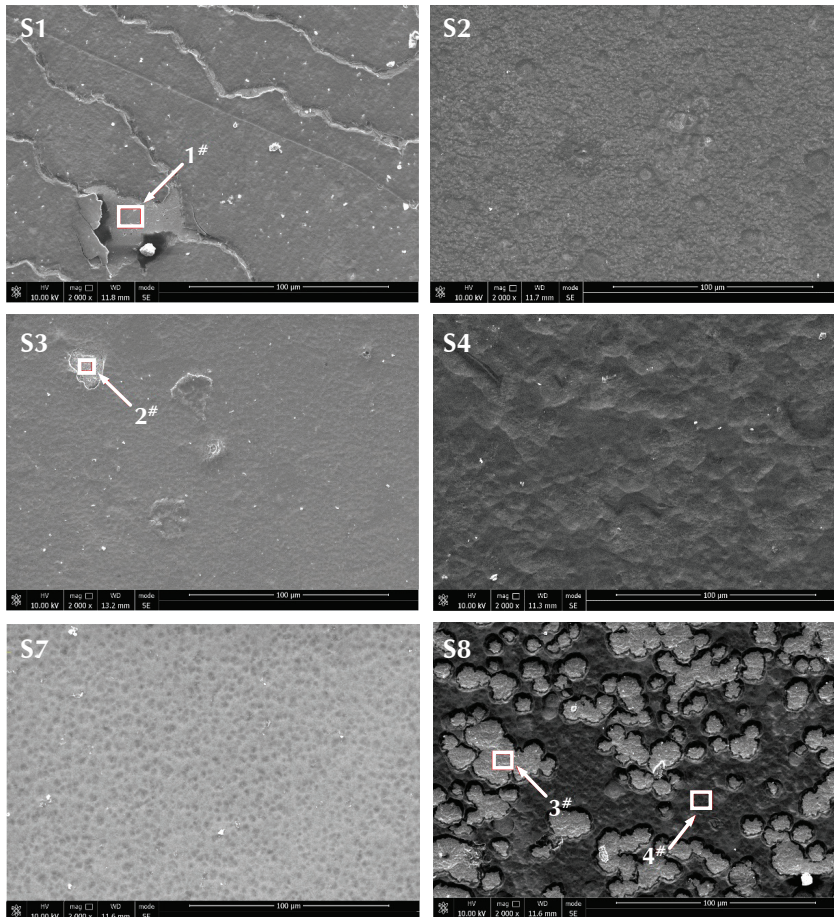
Fig. 1 – Typical surface micrographs of ion sputtering coating samples (unoxidized coatings)
Slika 1 – Karakteristični površinski mikrografi uzoraka premaza prskajućim ionima (neoksidiranih premaza)

The EDS analysis of points 1# and 2# in Fig. 2 shows that the coatings are peeled off. These results indicate that the ion bombardment under high source electrode voltage of 800 V can produce compressive stress, which plays an important role in the process of spalling.[23]

However, the coatings of S2, S4, S7 and S8 are very dense, uniform, and compact to the substrate without any cracks and defects. The above-discussed experiments demonstrate that two main factors play important roles in the deposition progress: one is the source electrode voltage resulting in the increase in ion quantity and velocity; the other is the parallel distance between the source electrode and the substrate.

Two different areas (black and white) in sample S8 were analysed by EDS. It can be found from the EDS analyses of points 3# and 4# that the average compositions of the two areas are similar. The existence of oxygen element in the unoxidized species indicates that various source material atoms, such as O^{2+}, O^-, and O^{2-}, come from the sputtering of the complex target includ-

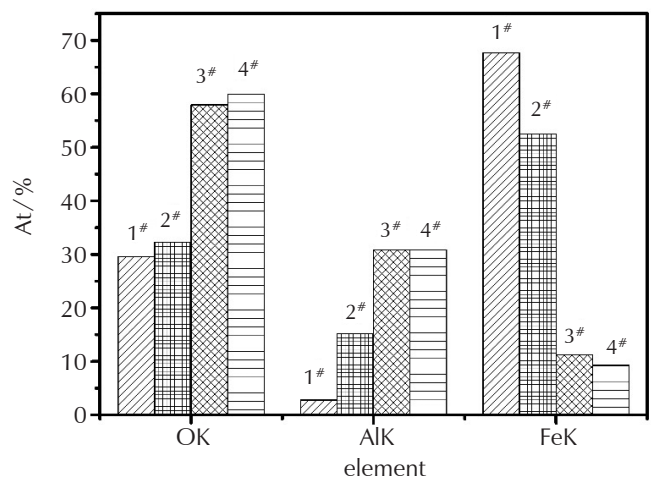ing α-Al₂O₃ seeds in the double glow plasmas discharge process.

Fig. 2 – EDS analysis of the sputter-deposited coatings
Slika 2 – EDS-analiza prskajuće raspoređenih premaza

Al/α-Al$_2$O$_3$ prepared with optimum parameters

Fig. 3 shows the phase and morphology of the coating prepared with optimum parameters. From Fig. 3(a), it can be found that the FeAl and Fe$_3$Al intermetallic compounds are the predominant phases in the unoxidized specimen, mainly caused by the diffusion of Al element into substrate promoted by heating the workpiece. Besides FeAl and Fe$_3$Al, a small amount of α-Al$_2$O$_3$ is detected, which means that the α-Al$_2$O$_3$ doped in the target is deposited on the substrate owing to energetic ion bombardment.

The coating is continuous and compact with no visible metallurgy flaw as shown in Fig. 3(b). From Fig. 3(c), the thickness of unoxidized coating was measured at about 11.6 µm. Considering the total deposition time of 3 h, the deposition rate was calculated to be about 64 nm min^{-1}. Compared with P. Jin's study,[14] the coatings in this study have faster growth speed. It is beneficial to promote depositing efficiency and surface quality of the coatings by supplying different bias voltage between the target and substrates.[24]

Oxidation

The coatings with the optimum parameters were further plasma oxidized under different oxygen flow. The GAXRD patterns of the oxidized coatings are shown in Fig. 4. After oxidation, the Al$_2$O$_3$ phase and Fe$_2$O$_3$ phase were detected in the sample. The result also indicates that there are two types of Al$_2$O$_3$ phase: α-Al$_2$O$_3$ and γ-Al$_2$O$_3$. When the oxygen flow is 0.5 sccm, some FeAl phase is left in the coating after oxidization, indicating that the FeAl phase cannot be completely oxidized with insufficient oxygen. As the oxygen flow increases, the peak intensity of γ-Al$_2$O$_3$ decreases while the peak intensity of α-Al$_2$O$_3$ increases. The relative phase ratio can be calculated by comparing the areas under peaks in the XRD pattern.[25]

$$R_{\alpha\text{-Al}_2\text{O}_3} = \frac{I_{\alpha\text{-Al}_2\text{O}_3}}{I_{\alpha\text{-Al}_2\text{O}_3} + I_{\gamma\text{-Al}_2\text{O}_3}} \tag{1}$$

where $I_{\alpha\text{-Al}_2\text{O}_3}$ and $I_{\gamma\text{-Al}_2\text{O}_3}$ are the integrated intensity of the highest peak of α-Al$_2$O$_3$ and γ-Al$_2$O$_3$, respectively. As the
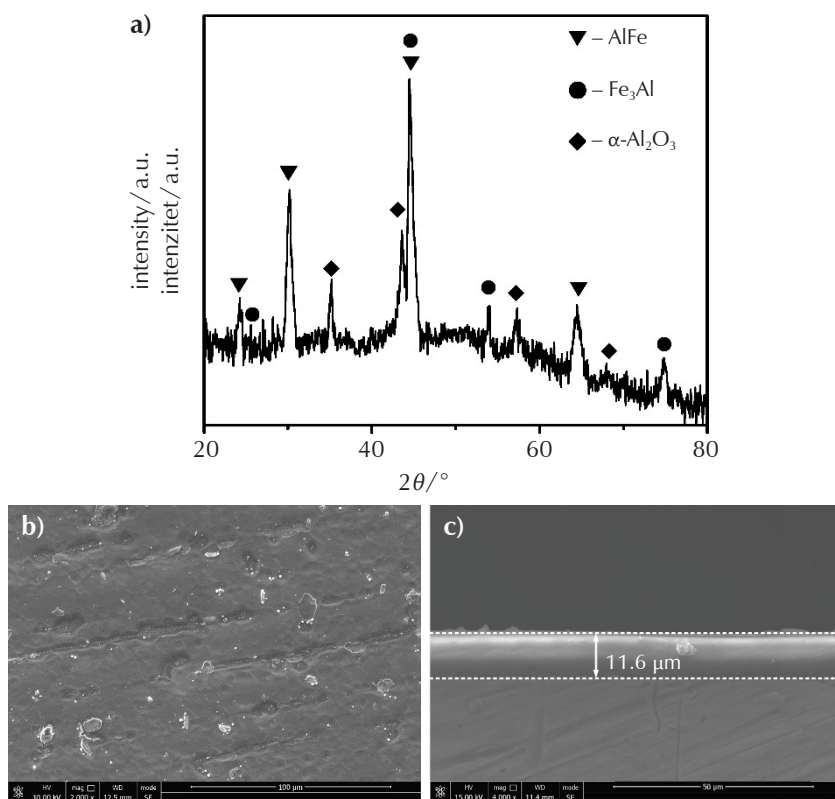

Fig. 3 – Phase and morphology of the coating with optimum parameters: (a) GAXRD pattern of the Al/α-Al$_2$O$_3$ coating, (b) Top-view of scanning electron micrographs, (c) Cross-section of scanning electron micrographs.
Slika 3 – Faza i morfologija premaza s optimalnim parametrima: (a) GAXRD-uzorak premaza Al/α-Al$_2$O$_3$, (b) pogled odozgo na skenirajuće elektronske mikrografe, (c) poprečni presjek skenirajućih elektronskih mikrografa.

oxygen flow increases, the formation of α-Al₂O₃ is promoted and the relative contents of α-Al₂O₃ are about 64.8 %, 66.2 %, 66.5 %, and 68.6 %, respectively. As we know, alpha phase transition of Al₂O₃ includes nucleation and growth process.[26] The addition of fine α-Al₂O₃ seeds provides a large number of nuclei for α-Al₂O₃ formation and reduces the energy barrier required for nucleation in the thermally activated process. Meanwhile, the high energetic ion bombardment can accelerate the mobility of the surface species and provide the α-Al₂O₃ formation energy.
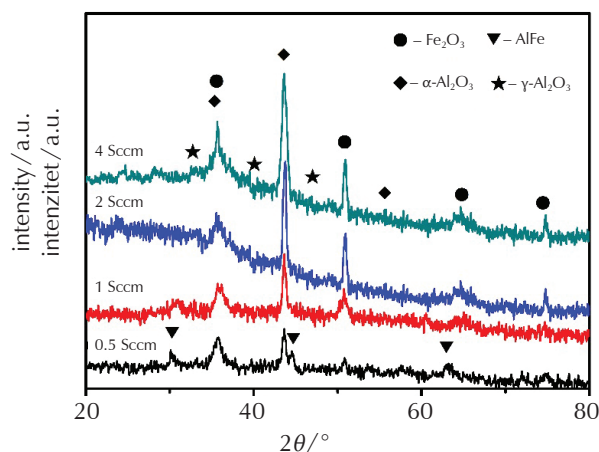

Fig. 4 – GAXRD pattern of the oxidized coatings with different oxygen flow

Slika 4 – GAXRD-uzorak premaza oksidiranih različitim protokom kisika

The surface morphology of the coatings oxidized with different oxygen flow is shown in Fig. 5. The surface morphology of the coating has no obvious change when the oxygen flow is 0.5 sccm (Fig. 5(a)). As shown in the Fig. 5(b) and (c), the dense and well-bonded coatings are obtained with the increase in oxygen flow. According to the Volmer-Weber mode,[27] stable nucleus can capture atoms both diffused from the surface of substrate and sputtered from the target, leading to the increment of the grain size. Numerous growing grains make isolated α-Al₂O₃ island grow into continuous coatings. From the magnified image of Fig. 4(b) and (c), the α-Al₂O₃ island consists of many circular particles. When further increasing the oxygen flow to 4 sccm, the coating is partly spalling.

Corrosion property

The polarization curves of 316 L and oxidized layers with different oxygen flow in 3.5 % NaCl solution are shown in Fig. 6. The corrosion potential and corrosion current are calculated in Table 4. The porosity of the coatings *P* is calculated as the corrosion current ratio of coatings and substrates.[28]

$$P = \frac{i_{corr}}{i^{\circ}_{corr}} \qquad (2)$$

where i_{corr} is the corrosion current of the oxidized coating and i°_{corr} is the corrosion current of the 316 L stainless steel. The higher the corrosion potential is, the stronger is the resistance to corrosion. At the same time, corrosion
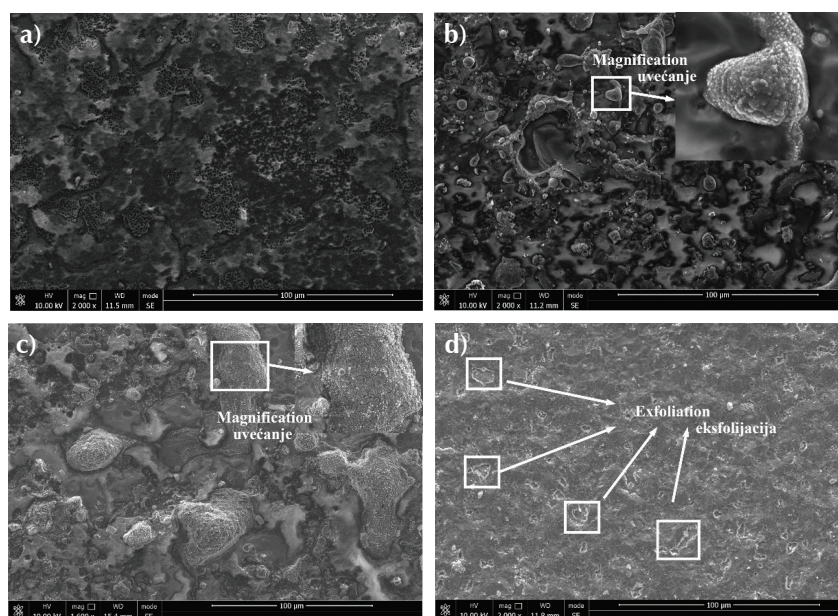

Fig. 5 – Surface morphology of the coating with different oxygen flow:
(a) 0.5 sccm, (b) 1 sccm, (c) 2 sccm, (d) 4 sccm.

Slika 5 – Površinska morfologija premaza s različitim protokom kisika:
(a) 0.5 sccm, (b) 1 sccm, (c) 2 sccm, (d) 4 sccm.

current is in proportion to the corrosion rate of materials. The smaller the corrosion current is, the better is the corrosion resistance performance. According to the curves, the polarization curves of alumina coatings shift upward to a more notable potential, suggesting that the alumina coatings are effective in the corrosion protection of the stainless steel substrate by reducing the corrosion current density and increasing the passive region.

In comparison with previously reported work,[24] in which alumina coatings with fraction of $w = 60\ \%$ exhibit the corrosion potential of −0.291 V, we obtain the minimum corrosion potential of sample 3 of −0.206 V which is better due to the following two reasons. Firstly, a relatively high content of α-Al$_2$O$_3$ in the coating is beneficial to improving corrosion resistance of the substrate.[29] Secondly, the dense alumina coating with millions of tiny particles may act as a barrier to block the diffusion of the aggressive media. With the calculation formula,[30] the lowest porosity of the coatings is 0.13 %.
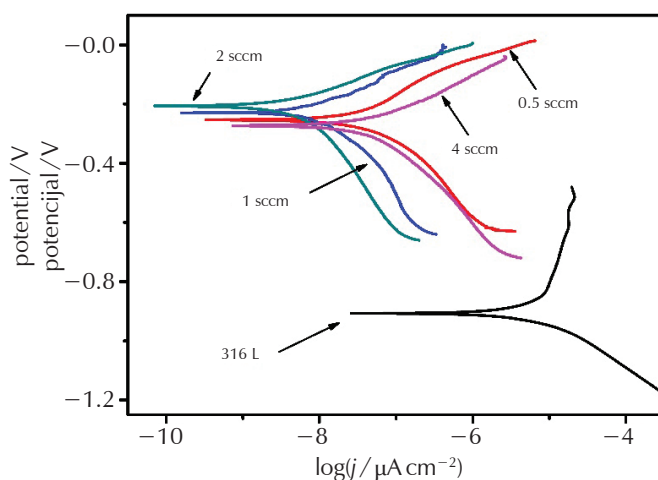

Fig. 6 – Polarization curves of composite coatings and 316 L stainless steel

Slika 6 – Polarizacijske krivulje kompozitnih premaza i nehrđajućeg čelika 316 L

Table 5   – Potentiodynamic polarization parameters of coatings and 316 L stainless steel
Tablica 5 – Potenciodinamička polarizacija parametara premaza i nehrđajućeg čelika 316 L

Samples Uzorci	Oxygen flow / sccm Protok kisika / sccm	Corrosion potential / V Korozijski potencijal / V	Corrosion current density / μA · cm^{-2} Gustoća korozijske struje / μA · cm^{-2}	Porosity / % Poroznost / %
1	0.5	−0.253	0.045	4.84
2	1	−0.231	0.022	0.24
3	2	−0.206	0.012	0.13
4	4	−0.272	1.087	11.6
316 L	–	−0.907	9.3	–

Conclusions

The influence of deposition parameters (including working pressure, source electrode, workpiece electrode and parallel distance) on the deposition rate were investigated by orthogonal array design. The parallel distance between the source electrode and the substrate was the most prominent factor which significantly influenced the thickness of the films. The optimum parameters were: working pressure, 30 Pa; source electrode voltage, 700 V; workpiece electrode voltage, 300 V; and the parallel distance between the source electrode and the substrate, 15 mm. Under optimized deposition conditions, dense and thick α-Al$_2$O$_3$ coatings were obtained by double glow plasma technique at 580 °C. The thickness of the coatings reached about 11.6 μm at the deposition rate of ~64.4 nm min^{-1}. It was found that iron aluminide formed at the interface between the coatings and the substrates. When applying further plasma oxidation, the formation of α-Al$_2$O$_3$ was promoted as oxygen flow increased. The oxidized coatings with the lowest porosity of about 0.13 % had the relative content of α-Al$_2$O$_3$ as high as 66.5 % when the oxygen flow was 2 sccm.

List of abbreviations and symbols
Popis kratica i simbola

sccm — standard cubic centimetre per minute; a flow equivalent to 1 cm³ min⁻¹ at T = 273.15 K and p = 1 bar
— standardni kubni centimetar po minuti; protok ekvivalentan 1 cm³ min⁻¹ pri T = 273,15 K i p = 1 bar

P — porosity of the coatings
— poroznost premaza

$R_{\alpha\text{-}Al_2O_3}$ — relative phase ratio
— relativan fazni omjer

References
Literatura

1. *S. Ruppi,* Deposition, microstructure and properties of texture-controlled CVD α-Al₂O₃ coatings, Int. J. Refract. Met. H. **23** (2005) 306–316, doi: http://dx.doi.org/10.1016/j.ijrmhm.2005.05.004.

2. *C. H. Zhou, J. Xu, S.Y. Jiang,* Reactive sputter deposition of alumina films on magnesium alloy by double cathode glow-discharge plasma technique, Mater. Charact. **61** (2010) 249–256, doi: http://dx.doi.org/10.1016/j.matchar.2009.12.007.

3. *X. X. Zhong, Y. Liu, J. Li, Y. W. Wang,* Structure and magnetic properties of FeSiAl-based soft magnetic composite with AlN and Al₂O₃ insulating layer prepared by selective nitridation and oxidation, J. Magn. Magn. Mater. **324** (2012) 2631–2636, doi: http://dx.doi.org/10.1016/j.jmmm.2012.03.026.

4. *Y. M. Chung, M. J. Jung, K. H. Nam, J. G. Han, S. H. Baeg, S. H. Yang,* A study on formation of Al and Al₂O₃ on the porous paper by DC magnetron sputtering, Surf. Coat. Tech. **171** (2003) 65–70, doi: http://dx.doi.org/10.1016/S0257-8972(03)00237-8.

5. *X. X. Ma, Y. D. He, D. R. Wang, J. Zhang,* Superior high-temperature oxidation resistance of a novel (Al₂O₃–Y₂O₃)/Pt laminated coating, Appl. Surf. Sci. **258** (2012) 4733–4740, doi: http://dx.doi.org/10.1016/j.apsusc.2012.01.069.

6. *R. G. Song,* Hydrogen permeation resistance of plasma-sprayed Al₂O₃ and Al₂O₃–13wt.% TiO₂ ceramic coatings on austenitic stainless steel, Surf. Coat. Tech. **168** (2003) 191–194, doi: http://dx.doi.org/10.1016/S0257-8972(03)00002-1.

7. *P. K. Sharm, V. V. Varadan, V. K. Varadan,* A critical role of pH in the colloidal synthesis and phase transformation of nano size α-Al₂O₃ with high surface area, J. Eur. Ceram. Soc. **23** (2003) 659–666, doi: http://dx.doi.org/10.1016/S0955-2219(02)00191-7.

8. *S. Cava, S. M. Tebcherani, S. A. Pianaro, C. A. Paskocimas, E. Longo, J. A. Varela,* Structural and spectroscopic analysis of γ-Al₂O₃ to α-Al₂O₃-CoAl₂O₄ phase transition, Mater. Chem. Phys. **97** (2006) 102–108, doi: http://dx.doi.org/10.1016/j.matchemphys.2005.07.057.

9. *T. S. Wang, J. Pu, C. Bo, L. Jian,* Sol–gel prepared Al₂O₃ coatings for the application as tritium permeation barrier, Fusion. Eng. Des. **85** (2010) 1068–1072, doi: http://dx.doi.org/10.1016/j.fusengdes.2010.01.021.

10. *J. Muller, M. Schierling, E. Zimmermann,* Chemical vapor deposition of smooth α-Al₂O₃ films on nickel base super alloys as diffusion barriers, Surf. Coat. Tech. **16** (1999) 120–125.

11. *I. Hideshima, T. Hosoi, T. Shimura, H. Watanabe,* Al₂O₃/GeO₂ stacked gate dielectrics formed by post-deposition oxidation of ultrathin metal Al layer directly grown on Ge substrates, Curr. Appl. Phys. **12** (2012) S75-S78, doi: http://dx.doi.org/10.1016/j.cap.2012.04.007.

12. *Y. Y. Takamura, F. Koch, H. Maier, H. Bolt,* Characterization of α-phase aluminum oxide films deposited by filtered vacuum arc, Surf. Coat. Tech. **142-144** (2001) 260–264, doi: http://dx.doi.org/10.1016/S0257-8972(01)01206-3.

13. *E. Wallin, T. I. Selinder, M. Elfwing,* Synthesis of α-Al₂O₃ thin films using reactive high-power impulse magnetron sputtering, Europhysics. Lett. **36** (2008) 82–86.

14. *P. Jin, G. Xu, M. Tazawa, K. Yoshimura, D. Musica, J. Alami, U. Helmersson,* Low temperature deposition of α-Al₂O₃ thin films by sputtering using a Cr₂O₃ template, J. Vac. Sci. Technol. A. **20** (2002) 2134–2136, doi: http://dx.doi.org/10.1116/1.1513641.

15. *J. M. Andersson, E. Wallin, U. Helmersson, U. Kreissig, E. P. Münger,* Phase control of Al₂O₃ thin films grown at low temperatures, Thin. Solid. Films. **513** (2006) 57–59, doi: http://dx.doi.org/10.1016/j.tsf.2006.01.016.

16. *J. Xu, J. Tao, Z. Y. Chen, W. H. Zhu, S. Y. Jiang, Z. Xu,* Preparation of Ni–Cu–Mo–Cr film deposited on AZ31 magnesium alloy by double glow sputtering with Cu interlayer, Surf. Coat. Technol. **202** (2007) 577–582, doi: http://dx.doi.org/10.1016/j.surfcoat.2007.06.034.

17. *Y. B. Lin, C. Wang, J. Tao,* Induction effect of α-Al₂O₃ seeds on formation of alumina coatings prepared by double glow plasma technique, Surf. Coat. Tech. **235** (2013) 544–551, doi: http://dx.doi.org/10.1016/j.surfcoat.2013.08.022.

18. *G. S. Zhong, X. F. Guo, S. H. Zhang, Y. S. Zhen,* Optimization of the assembly efficiency for lidamycin chromophore bound to its apoprotein: a case study using orthogonal array, Biomed. Environ. Sci. **24**(6) (2011) 602–607.

19. *L. F. Lai, W. J. Zeng, X. Z. Fu, R. Sun, R. X. Du,* Optimization of sputtering parameters for NiCr alloy deposition on copper foil as embedded thin film resistor, Surf. Coat. Tech. **218** (2013) 80–86, doi: http://dx.doi.org/10.1016/j.surfcoat.2012.12.030.

20. *J. P. Horiguchi, S. Kobayashi, Y. Yamazaki, T. Nakanishi, D. Itabashi, K. Omata, M. Yamada,* Optimization of K–Ni/α-Al₂O₃ catalyst for high-pressure oxidative reforming of methane by radial basis function network and multivariate analysis. Appl. Catal. A-GEN. **377** (2010) 9–15, doi: http://dx.doi.org/10.1016/j.apcata.2009.12.041.

21. *L. Shen, L. Wang, J. J. Xu,* Plasma nitriding of AISI 304 austenitic stainless steel assisted with hollow cathode effect. Surf. Coat. Tech. **228** (2013) S456–S459, doi: http://dx.doi.org/10.1016/j.surfcoat.2012.05.026.

22. *Y. C. Zhou, T. Hashida,* Coupled effects of temperature gradient and oxidation on thermal stress in thermal barrier coating system. Int. J. Solids. Struct. **38** (2001) 4235–4264, doi: http://dx.doi.org/10.1016/S0020-7683(00)00309-7.

23. *W. G. Mao, Y. C. Zhou, L. Yang, X. H. Yu,* Modeling of residual stresses variation with thermal cycling in thermal barrier coatings. Mech. Mater. **38** (2006) 1118–1127, doi: http://dx.doi.org/10.1016/j.mechmat.2006.01.002.

24. *H. B. Liu, J. Tao, J. Xu, Z. F. Chen, X. Y. Luo,* Microstructure and mechanical properties of alumina coatings prepared by double glow plasma technique, Appl. Surf. Sci. **256** (2010) 5939–5945, doi: http://dx.doi.org/10.1016/j.ap-

susc.2010.03.083.

25. *S. Kumara, K. Kang, B. Gyuyeol, V. Selvarajan, C. Lee,* Synthesis and characterization of alumina nano-powders by oxidation of molten aluminium in a thermal plasma reactor: Comparison with theoretical estimation, Mater. Chem. Phys. **112**(2) (2008) 436–441, doi: http://dx.doi.org/10.1016/j.matchemphys.2008.05.070.

26. *K. Yang, J. W. Feng, X. M. Zhou, S.Y. Tao,* In-situ formed γ-Al$_2$O$_3$ nanocrystals repaired and toughened Al$_2$O$_3$ coating prepared by plasma spraying, Surf. Coat. Tech. **206** (2012) 3082–3087, doi: http://dx.doi.org/10.1016/j.surfcoat.2011.12.014.

27. *V. I. Perekrestov, Yu. O. Kosminska, A. S. Kornyushchenko, V. M. Latyshev,* Self-organization of copper nanosystems under Volmer-Weber condition during quasi-equilibrium condensation, Physica B. **411** (2013) 140–148, doi: http://dx.doi.org/10.1016/j.physb.2012.11.036.

28. *H. G. Yang, X. M. Zhu, M. K. Lei,* Evaluation of porosity of hard coatings by corrosion electrochemistry, Corros. Sci. Prot. Technol. **17** (2005) 413–417.

29. *S. D. Mao, H. X. Yang, F. Huang, T. T. Xie, Z. L. Song,* Corrosion behavior of sintered NdFeB coated with Al/Al$_2$O$_3$ multilayers by magnetron sputtering, Appl. Surf. Sci. **257** (2011) 3980–3984, doi: http://dx.doi.org/10.1016/j.apsusc.2010.11.162.

30. *H. G. Yang, X. M. Zhu, M. K. Lei,* Evaluation of porosity of hard coatings by corrosion electrochemistry, Corros. Sci. Prot. Tech. **17** (2005) 413–417.

SAŽETAK

Optimizacija parametara taloženja za premaze α-Al$_2$O$_3$ tehnikom plazme dvostrukog sjaja

Yuebin Lin,[a,b] Yizhou Shen,[a] Tengfei Chen[a] i Jie Tao[a]*

Za dobivanje gustih i debelih premaza α-Al$_2$O$_3$ na nehrđajućem čeliku 316 L pri niskoj temperaturi od 580 °C parametri za pripravu premaza α-Al$_2$O$_3$ optimirani su tehnikom plazme dvostrukog sjaja. Udaljenost između izvora elektrode i supstrata, radni tlak, napon izvorne elektrode i napon elektrode radnog komada dobiveni su metodom ortogonalnog niza L9. Debljina, mikrostruktura, kemijski sastav i fazne komponente pršteći pohranjenih premaza Al/α-Al$_2$O$_3$ analizirani su pomoću 3-D beskontaktne površinske analize, skenirajućom elektronskom mikroskopijom opremljenom spektrometrijom disperzije energije rendgenskog zračenja i difrakcijom kuta sjaja rendgenskog zračenja. Rezultati su pokazali da usporedna udaljenost između izvora elektrode i supstrata ima dominantnu ulogu u određivanju debljine filmova. Premazi pripravljeni pri optimalnim uvjetima pokazali su vrlo gustu, ujednačenu i kompaktnu mikrostrukturu bez pukotina i oštećenja. Utvrđeno je da je na granici između premaza i supstrata formiran željezov aluminid. Debljina premaza je pri stopi taloženja od ∼64,4 nm min⁻¹ dosegla oko 11,6 μm. Ako je protok kisika 2 sccm, oksidirani premazi s najmanjom poroznošću od oko 0,13 % imaju relativni udjel α-Al$_2$O$_3$ od oko 66,5 %.

Ključne riječi
Tehnika plazme dvostrukog sjaja, premazi α-Al$_2$O$_3$, niska temperatura, optimizacija

[a] College of Material Science and Technology, Nanjing University of Aeronautics and Astronautics, 29 Yudao Street, 210 016 Nanjing, Kina

[b] Jiangsu Provincial Key Laboratory for Interventional Medical Devices, Huaiyin Institute of Technology, 1 Meicheng Street, 223 003 Huaian, Kina